AGU ADVANCING EARTH AND SPACE SCIENCE

Geophysical Research Letters

RESEARCH LETTER
10.1029/2021GL093566

Key Points:

- We provide the first observational and modeling evidence of a cold ion wake downstream of the Moon when located in Earth's magnetotail lobes
- Using the Moon as a natural solar shield, we reveal an otherwise hidden, cold ion population that may originate from Earth's ionosphere
- The lunar plasma environment in the terrestrial magnetotail lobes provides a link to the plasma interactions at outer solar system moons

Correspondence to:
L. Liuzzo,
liuzzo@berkeley.edu

Citation:
Liuzzo, L., Poppe, A. R., Halekas, J. S., Simon, S., & Cao, X. (2021). Investigating the Moon's interaction with the terrestrial magnetotail lobe plasma. *Geophysical Research Letters*, *48*, e2021GL093566. https://doi.org/10.1029/2021GL093566

Received 26 MAR 2021
Accepted 26 APR 2021

Investigating the Moon's Interaction With the Terrestrial Magnetotail Lobe Plasma

Lucas Liuzzo[1], Andrew R. Poppe[1], Jasper S. Halekas[2], Sven Simon[3], and Xin Cao[2]

[1]Space Sciences Laboratory, University of California, Berkeley, CA, USA, [2]Department of Physics and Astronomy, University of Iowa, Iowa City, IA, USA, [3]School of Earth and Atmospheric Sciences, Georgia Institute of Technology, Atlanta, GA, USA

Abstract We present observations of the Moon's plasma interaction in Earth's magnetotail lobes by the ARTEMIS mission, and compare these to hybrid model results to constrain the global properties of the lunar electromagnetic environment. We identify, for the first time in the magnetotail lobes, a low-energy wake extending multiple lunar radii downstream of the Moon along the ambient flow direction. This wake is tilted out of the lunar optical shadow, allowing for detection of the otherwise unobservable cold ambient magnetospheric plasma. Similar eclipse encounters may provide additional opportunities to measure this low-energy plasma potentially originating from the terrestrial ionosphere. We find lunar ionospheric outflow extending multiple Moon radii downstream that generates asymmetries in the Moon's plasma environment and shares characteristics with the plasma interactions of Rhea, Tethys, and Dione. The extensive ARTEMIS data set may therefore provide additional insights into the plasma environments near moons of the outer solar system.

Plain Language Summary Earth's Moon is exposed to a wide range of particle and magnetic field environments during its 29.5-day orbit. When outside of Earth's magnetosphere, the Moon experiences the rapidly flowing, dense solar wind plasma. However, for a few days each month, the terrestrial magnetosphere shields the Moon from the solar wind; instead, it is exposed to the low-density plasma within Earth's magnetotail lobes. For these conditions, we report observations from the Acceleration, Reconnection, Turbulence, and Electrodynamics of the Moon's Interaction with the Sun (ARTEMIS) spacecraft orbiting the Moon. By modeling the Moon's plasma interaction in the lobes, we find that dense, lunar ionospheric particles drastically perturb the local plasma environment, similar to moons in the outer solar system. On the nightside, we provide the first observation of an extended, cold plasma wake tilted out of the Moon's optical shadow. This geometry allowed ARTEMIS to measure an otherwise invisible, ambient magnetospheric ion population that is responsible for shaping the lunar plasma interaction. Hence, the Moon acts as a natural filter for plasma observations in the Earth's magnetotail, an effect that may therefore be used to understand loss processes of Earth's ionospheric plasma.

1. Introduction

While not surrounded by an appreciable global atmosphere, Earth's Moon (radius $R_L = 1{,}737.4$ km) possesses a tenuous neutral exosphere composed of multiple species reaching a surface density on its sunlit hemisphere of 10^4–10^5 cm^{-3} (e.g., R. Hodges et al., 1974; R. R. Hodges, 1975; Potter & Morgan, 1988; Stern, 1999; Benna et al., 2015). This exosphere is ionized mainly by photoionization, with minor contributions from charge exchange and electron impacts (Sarantos et al., 2012). The resulting ionosphere extends to 100s of km in altitude with peak densities below ~1 cm^{-3} (Halekas et al., 2018), although highly localized enhancements in the ionospheric near-surface number density have been reported on smaller scales (~10s of km; e.g., Imamura et al., 2012; Choudhary et al., 2016).

During its orbit, the Moon experiences a wide range of plasma environments. Outside of Earth's magnetosphere, the solar wind density exceeds that of the lunar ionosphere by over an order-of-magnitude. Hence, the ionosphere acts as test-particles embedded within the local electromagnetic fields (e.g., Halekas et al., 2012). In this environment, an extended plasma cavity forms downstream of the Moon (Kallio, 2005; Michel, 1968; Ness, 1965; Ogilvie et al., 1996; Zhang et al., 2014). Within Earth's magnetotail lobes, however,

the density of the lunar ionosphere often exceeds the local plasma density by over an order-of-magnitude (Harada et al., 2013; Poppe et al., 2012; Tanaka et al., 2009). Hence, these ions significantly contribute to mass- and momentum-loading of the ambient magnetospheric plasma, thereby perturbing the local electromagnetic fields (Cao et al., 2020). However, the global structure of the lunar plasma interaction within the unique environment of the terrestrial magnetotail remains largely unconstrained. Additionally, despite numerous observations of an extended wake forming downstream of the Moon when located within the solar wind, the existence and characteristics of a plasma wake within the tenuous magnetotail lobes is unknown.

We report the first observations of a lunar wake within the terrestrial magnetotail lobes during individual encounters by the Acceleration, Reconnection, Turbulence, and Electrodynamics of the Moon's Interaction with the Sun (ARTEMIS) mission (Angelopoulos, 2011). By taking advantage of the Moon's optical shadow and active spacecraft potential control on the ARTEMIS probes, we detect a hidden, cold and tenuous ambient magnetotail plasma, possibly of terrestrial origin, that is typically unobservable in such low-density environments (e.g., Seki et al., 2003; Engwall, Eriksson, Cully, André, Puhl-Quinn, et al., 2009). By modeling the lunar plasma interaction in the magnetotail lobes, we characterize the Moon's cold ion wake and identify two "wings" generated by plasma absorption that extend from the lunar surface. Constraining the Moon's electromagnetic environment during these rather uncommon conditions reveals surprising similarities to multiple Saturnian moons.

2. ARTEMIS Observations

ARTEMIS consists of two identically instrumented probes (P1, P2) orbiting the Moon along highly elliptical, asynchronous trajectories (Angelopoulos, 2011). Here, we present ARTEMIS observations of the lunar plasma environment for two days while embedded within the low-density terrestrial magnetotail lobes (see Figure 1).

2.1. October 30, 2012: Observations

Figures 1a–1g shows ARTEMIS observations of the lunar environment on October 30, 2012, while the Moon was far downstream of the Earth within the nominal location of the terrestrial magnetotail (figure 1(a)). The magnetosphere was quiescent, with daily Ap and maximum Kp indices of 2 and 1, respectively. Between 04:45 and 09:15 UT, P1 traveled from the dawn, anti-sunward flank of the Moon, crossed the lunar optical shadow from $-4.8R_L$ to $-2.3R_L$ downstream, passed through periselene at an altitude of $0.23R_L$ and lunar local time 15:40 h, and transited across the lunar dayside hemisphere (figure 1(b)). During this same time period, P2 remained at radial distances ranging from 4.8 to $9.1R_L$. Figures 1(c–g) show the P1 magnetic field, P1 and P2 ion energy spectra, P1 ion velocity, and P1 plasma number density, respectively. The magnetospheric field predominantly pointed earthward (i.e., $+x$ SSE), indicative of the Moon's position within the northern terrestrial magnetotail lobe. In the Moon-centered SSE (Selenocentric Solar Ecliptic) system, $+z$ is parallel to the (upward) normal to Earth's ecliptic plane and $+y$ completes the right-handed set (approximately anti-aligned with the Moon's orbital motion). Note that during the P1 lunar shadow crossing between 05:54–07:16 UT, the magnetic field B_y and B_z components show deviations on the order of +2 nT and −1 nT, respectively. These features are *not* geophysical in nature, but rather due to incomplete despinning of the ARTEMIS magnetic field vector while in shadow (for further details, see Georgescu et al., 2011).

Exposed to sunlight within the low-density magnetotail lobes, the ARTEMIS spacecraft potential typically rises to large values; here, between +25 and +65 V (red curves in figures 1(d–e)). These potentials repel ions from the Electrostatic Analyzer (ESA) instrument (McFadden, Carlson, Larson, Ludlam, et al., 2008), preventing ions at energies *below* the potential from being observed. However, during eclipses (caused by the Moon or the Earth), spacecraft photoemission naturally ceases. To prevent large, *negative* spacecraft potentials from developing (which would otherwise accelerate ions into the ESAs; see Bonnell et al., 2008; Halekas et al., 2011), ARTEMIS transitions from a "floating" to a "driven" spacecraft-potential mode using the Electric Field Instrument (EFI). The red curve in figure 1(d) shows this transition: ∼5 min before eclipse entry to ∼5 min after eclipse exit, the EFI probes actively maintain near-zero spacecraft potentials. Thus, while in eclipse, this driven spacecraft-potential mode allows low-energy ions to enter the ESAs with only minimal distortions to their distributions.

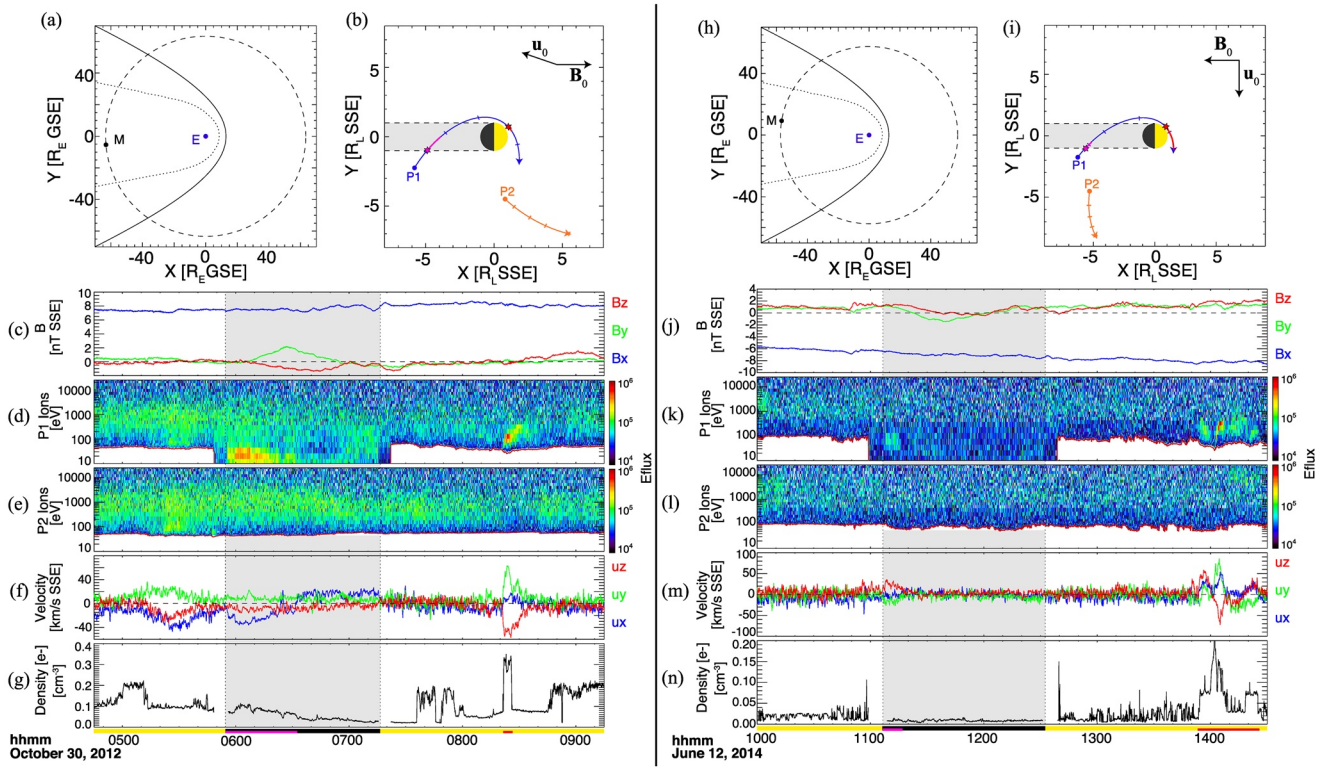

Figure 1. Lunar position, ARTEMIS trajectories, and observations on (a–g) October 30, 2012 from 04:45–09:15 and (h–n) June 12, 2014 from 10:00–14:30 (see text for further detail). Hash marks in figures (b) and (i) delineate 1 h intervals, and projections of the background flow and magnetic field vectors are included. Pink and red stars, and colored trajectory segments, highlight locations of the observed low-energy ambient plasma and pickup ion bursts, respectively. Gray shading and dashed lines denote the cylindrical lunar optical shadow. The bars below figures (g) and (n) illustrate when P1 was in (yellow) sunlight and (black) shadow, with pink and red regions corresponding to the segments in figures (b) and (i).

As seen in 1(d), ion fluxes remain near background count levels (figure 1(e)), with two exceptions. First, just after entering the lunar optical shadow, a population of cold ions with densities of ∼0.1 cm^{-3} and energies between 20 and 40 eV appears from 05:54 to 06:32 (pink star and trajectory segment in figure 1(b)). This population has a velocity in SSE coordinates of $\mathbf{u}_0 \approx \left[-30, +10, -10\right]$ km / s—primarily flowing down-tail along the field lines with a small perpendicular convective drift.

These "hidden" low-energy ions represent the ambient population near the Moon. Using its driven spacecraft-potential mode, P1 observed this otherwise invisible population for ∼37 min. However, during the remaining period within eclipse (06:32–07:16), these low-energy ions disappear, marking P1's entry into the cold plasma wake. As ARTEMIS moves to lower nightside altitudes, the ambient population is increasingly absorbed by the Moon and the probe detects a gradually decreasing density profile (figure 1(g)). Hence, the non-zero perpendicular flow velocity of the ambient, hidden ion population has shifted this plasma wake out of the Moon's optical shadow (by ∼25°). The Moon acts as a solar occultation disk, with these low-energy, ambient ions only revealing themselves within the lunar optical shadow, *before* ARTEMIS enters the tilted plasma wake.

The second notable feature is an ion burst at energies from 60–300 eV, appearing near 08:22 UT while P1 transits the lunar dayside (red star/segment in figure 1(b)). Here, the net ion velocity is mainly perpendicular to the magnetic field ($u_y > 0$, $u_z < 0$; figure 1(f)). We identify this increased flux as pickup ions from the lunar exosphere, based on previous, similar observations (e.g., Cao et al., 2020; Poppe et al., 2013, 2012; Zhou et al., 2013). These perpendicular ion velocities are consistent with gyration of newly born ions in a $+x$-aligned magnetic field, located near the top of their cycloidal arcs. A slight field-aligned ($u_x > 0$) component is also apparent during this period, likely indicating pickup ions that have interacted with the dayside

lunar electrostatic sheath, scattering ions parallel and perpendicular to the local magnetic field (Harada et al., 2013; Poppe et al., 2013).

2.2. June 12, 2014: Observations

Figures 1h–1n show ARTEMIS observations on June 12, 2014, during which the P1 probe traveled through the lunar optical shadow before passing within $0.16R_L$ of the dayside surface. Many features are similar to those on October 30, 2012: A quiescent magnetosphere (daily Ap = 4, maximum $Kp = 2$), the P1 trajectory, and the Moon's position within the terrestrial magnetotail lobes (albeit the southern lobe since $B_x < 0$; figure 1(j)). The ambient plasma density of $\sim 10^{-2}$ cm^{-3} was low, nearly an order-of-magnitude below the October 30, 2012 encounter (see figure 1(n)). The potential-corrected ion spectra (figures 1(k–l)) again show that upon entry into the lunar optical shadow, P1 detected the low-energy ambient ion population from 11:07 to 11:16 UT. In contrast to the previous encounter, the intensity of this population is much weaker, appearing over a shorter time interval without any field-aligned velocity ($\mathbf{u}_0 = \left[0, -20, +20\right]$ km / s; figure 1(m)).

P1 also observed higher energy ions correlated with passage across the lunar dayside from 13:53 to 14:25 UT. This observation again indicates newly born ionospheric ions, given large perpendicular velocities suggesting pickup ion gyration, and considering $\mathbf{u}_0 \perp \mathbf{B}_0$ (figure 1(i)). However, unlike on October 30, 2012 (cf. Figure 1f), the u_z component displays a sharp sign reversal. This, along with strong earthward velocities ($u_x > 0$), is further evidence that a portion of these pickup ions interacted with the dayside lunar photoelectron sheath before being detected (Poppe et al., 2013).

3. Hybrid Modeling of the Lunar Plasma Interaction

To understand the Moon's three-dimensional (3D) plasma interaction on these days and further characterize the ARTEMIS observations, we apply the Adaptive Ion-Kinetic, Electron-Fluid (AIKEF) hybrid model (Müller et al., 2011). AIKEF treats ions as particles and electrons as a massless, charge-neutralizing fluid. This approach is necessary to understand the Moon's interaction with the lobe plasma since the gyroradii of ionospheric particles may exceed the size of the Moon itself (e.g., Zhou et al., 2014). AIKEF has been successfully applied to understand magnetic field and plasma observations near multiple objects through-out the solar system (Liuzzo et al., 2017, 2018, 2019a, 2019b; Arnold, Liuzzo, & Simon, 2020; Arnold, Simon, & Liuzzo, 2020; Feyerabend et al., 2017) and to quantitatively reproduce features of the lunar-solar wind interaction (Vernisse et al., 2013; Wiehle et al., 2011). AIKEF is therefore well-suited for this study.

Each simulation obtains the ambient plasma conditions from observations during the respective ARTEMIS encounter, treating the Moon as a resistive, absorbing obstacle of radius R_L. For the October 30, 2012 simulation, we use an ambient number density $n_0 = 0.1$ cm^{-3} and total plasma beta $\beta_0 = 0.1$ (Figures 1a–1g), with an assumed upstream mass $m_0 = 1$ amu. In the SSE frame, we set the bulk plasma velocity to $\mathbf{u}_0 = \left[-30, +10, -10\right]$ km / s (i.e., that of the "hidden" ambient population), and use a constant, spatially homogeneous magnetic field of $\mathbf{B}_0 = \left[+8, +0, +0\right]$ nT. For the June 12, 2014 encounter, we set $n_0 = 0.03$ cm^{-3}, $\beta_0 = 0.02$, $m_0 = 1$ amu, $\mathbf{u}_0 = \left[0, -20, +20\right]$ km / s, and $\mathbf{B}_0 = \left[-7.5, +0, +0\right]$ nT (Figures 1h–1n). The magnetotail lobe plasma was remarkably sub-Alfvénic and subsonic on these two days, with Alfvénic and sonic Mach numbers of $M_A = 0.06$ and $M_s = 0.23$ (October 30, 2012), and $M_A = 0.02$ and $M_s = 0.14$ (June 12, 2014).

AIKEF represents the lunar exosphere via a barometric law that is rotationally symmetric about the $+x$ axis with a $\cos(\phi)$ dependence (with solar zenith angle ϕ) such that the terminator and nightside density is zero. We set the mean exospheric mass to 28 amu (Zhou et al., 2013), scale height to 100 km (Stern, 1999), and maximum subsolar surface number density to 10^4 cm^{-3} (Daily et al., 1977). This exosphere is ionized using a uniform ionization rate of 10^{-6} s^{-1} (Halekas et al., 2013). For these days, the maximum gyroradius of an ionospheric pickup ion with mass $m = 28$ amu is $\sim 1.5R_L$, thereby necessitating the hybrid approach. Each simulation uses a maximum grid resolution of $0.05R_L$ and 100 particles per cell, with a domain extending $\sim \pm 12R_L$ from the center of the Moon along each axis.

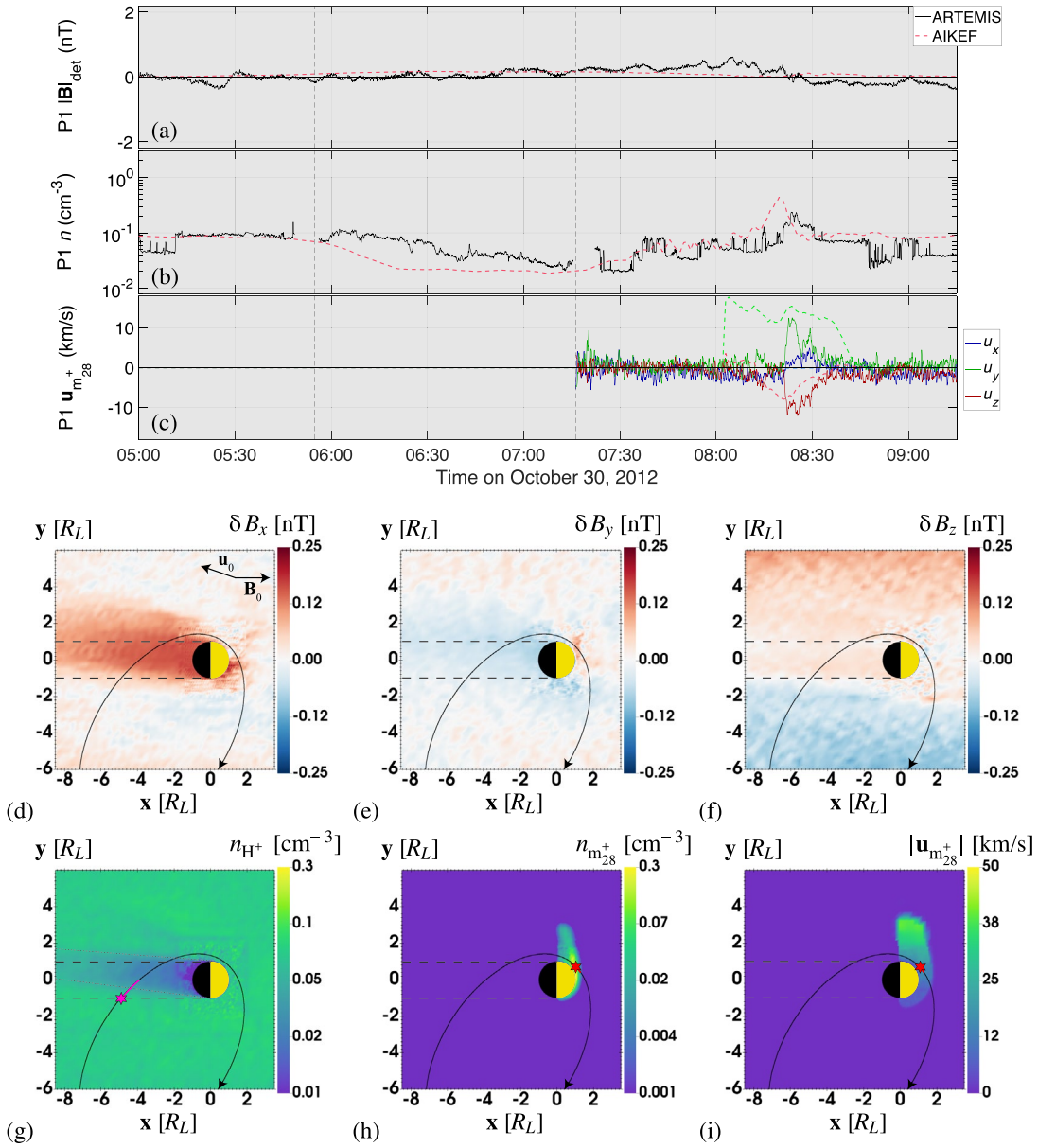

Figure 2. SSE magnetic field and plasma moments for the October 30, 2012 encounter. Quantities are described in the text. In figures (a–c), solid lines denote observations while dashed lines are model results. Vertical dashed lines delineate the lunar optical shadow. figures (d–i) display model results in the SSE *x-y* plane. The (solid) P1 trajectory and (dashed) lunar optical shadow are projected onto this plane. Dotted lines in figure (g) denote the location of the plasma wake. Stars and colored trajectory segments in figures (g–i) denote the location of the *observed* (pink) low-energy magnetotail population and (red) pickup ion burst.

3.1. October 30, 2012: Modeling

Figure 2a displays the detrended magnetic field magnitude along the P1 trajectory (solid line) observed by ARTEMIS and (dashed line) modeled by AIKEF for the October 30, 2012 encounter. On this day, both probes measured a gradual enhancement in |**B**| on scales much larger than the lunar interaction region (Figure 1a), which has been subtracted in Figure 2a to facilitate comparison with the model. Since the magnetic field despinning procedure within the optical shadow may leave residual phase errors in each magnetic field component (Georgescu et al., 2011), we present only the field magnitude, which is unaffected.

Figures 2b and 2c display the electron number density and pickup ion bulk velocity, respectively, during the encounter. Since lunar pickup ions were not detected until after P1 exited the shadow (viz. Figures 1a–1g),

we only include the observed ion velocity after that time. Since the ARTEMIS ESAs do not resolve mass, the pickup ion velocity is overestimated by ~ $\sqrt{28}$ (e.g., McFadden, Carlson, Larson, Bonnell, et al., 2008; Zhou et al., 2013). We correct for this factor in the ARTEMIS velocities in figure 2(c). Along the P1 trajectory, AIKEF reaches agreement with many of the observed quantities. Within the optical shadow, the magnetic field is nearly featureless besides slight, <0.1 nT fluctuations in the observed field. Outside of the shadow, the observed field reaches a maximum value of 0.4 nT, a factor of only ~1.3 larger than the modeled value. The densities within the shadow achieve similar minima; however, the modeled density decreases more rapidly—reaching its minimum near 06:20—and remains constant for ~1 h while the observed depletion occurs more gradually. These differences may be caused by a slightly greater lateral component of the ambient flow than assumed for the model, further shifting the plasma wake.

Figures 2(d–i) display the lunar plasma environment from the hybrid model in the SSE *x*-*y* plane. Perturbations above and below background are shown for the magnetic field components in figures 2(d–f). Figure 2(g) illustrates that magnetospheric plasma absorption in the ramside hemisphere causes a density wake ~$2R_L$ wide to form, extending >$8R_L$ downstream. Dotted lines in figure 2(g) illustrate this wake, highlighting its tilt out of the lunar optical shadow (horizontal dashed lines). Immediately upon entering the shadow, ARTEMIS observed the ambient magnetospheric plasma (pink stars/segments in figures 1(b) and 2(g)), before its disappearance upon entering the plasma cavity. P1 entered this wake further downstream of the Moon ($x \approx -5R_L$) compared to where it exited ($x \approx -2R_L$), contributing to the observed ramp-like density depletion (figure 2(b)).

To maintain pressure balance within this density cavity, the wakeside magnetic field is compressed, manifesting as an enhanced signature of δB_x confined to a cylinder ~$2R_L$ wide (figure 2(d)). Similar pressure balance features appear in the extended lunar wake when located in the solar wind (e.g., Fatemi et al., 2012; Halekas et al., 2005; Travnicek et al., 2005), and near moons in the outer solar system including Rhea and Dione (e.g., Khurana et al., 2017; Krupp et al., 2020; Roussos et al., 2008; Simon et al., 2012, 2011). The pickup ion populations of these Saturnian moons are so dilute that they are unable to compensate the reduced pressure caused by absorption of the magnetospheric plasma.

Although the Moon's ionospheric density exceeds the magnetotail lobe plasma by an order-of-magnitude (Figures 1d–1g and 2), lunar ions are *also* unable to contribute to pressure balance in the wakeside cavity during this encounter. Due to the nearly aligned orientation of the magnetospheric field and flow velocity, the $\mathbf{E} \times \mathbf{B}$ drift velocity is $\left[0,+10,-10\right]$km / s; that is, within a plane nearly perpendicular to the wake. This, combined with the location of the dayside lunar ionosphere and ion gyration about the +*x*-aligned magnetospheric field, results in pickup ions that unable to even *access* the downstream wake (see Figure 2h), let alone contribute to its pressure balance. Rather, the pressure is entirely compensated by the magnetic field. We can therefore estimate the maximum contribution of the lunar plasma interaction to the local field perturbations using an analytic formula. Applying the method of Simon et al. (2012)—which assumes complete evacuation of plasma in the wake—we find a maximum wake perturbation δB over the background field B_0 of

$$\delta B = B_0\left(\sqrt{\beta_0 + 1} - 1\right) \approx 0.4 \text{ nT}, \tag{1}$$

consistent with the ARTEMIS observation and the modeled $\delta B \approx 0.3$ nT (Figures 2a and 2d-2f).

On the dayside, the Moon's plasma environment is perturbed by the lunar ionosphere (Figures 2h and 2i). Modeled densities reach a peak surface value of 0.6 cm^{-3} and remain on the lunar dayside ($x > 0$). Such a spatially inhomogeneous, dense ion population may generate a system of "hemisphere coupling" currents, known from Saturn's moon Enceladus (Saur et al., 2007). The P1 probe encountered this pickup ion population after crossing the terminator, marked by a steadily increasing plasma density reaching $n \approx 0.25$ cm^{-3} just before 08:30, a factor of ~1.5 below the maximum modeled density (Figure 2b). At this time, P1 measured an enhanced perpendicular velocity (i.e., $u_y > 0$ and $u_z < 0$) and a burst of 100 eV ions at fluxes over an order-of-magnitude greater than in the ambient plasma (Figures 1d–1f). Figures 2(b–c) show that the magnitude and structure of the modeled number density and the u_z velocity, as well as the magnitude of the modeled u_y, agree with the ARTEMIS measurements of this pickup population. However, the width

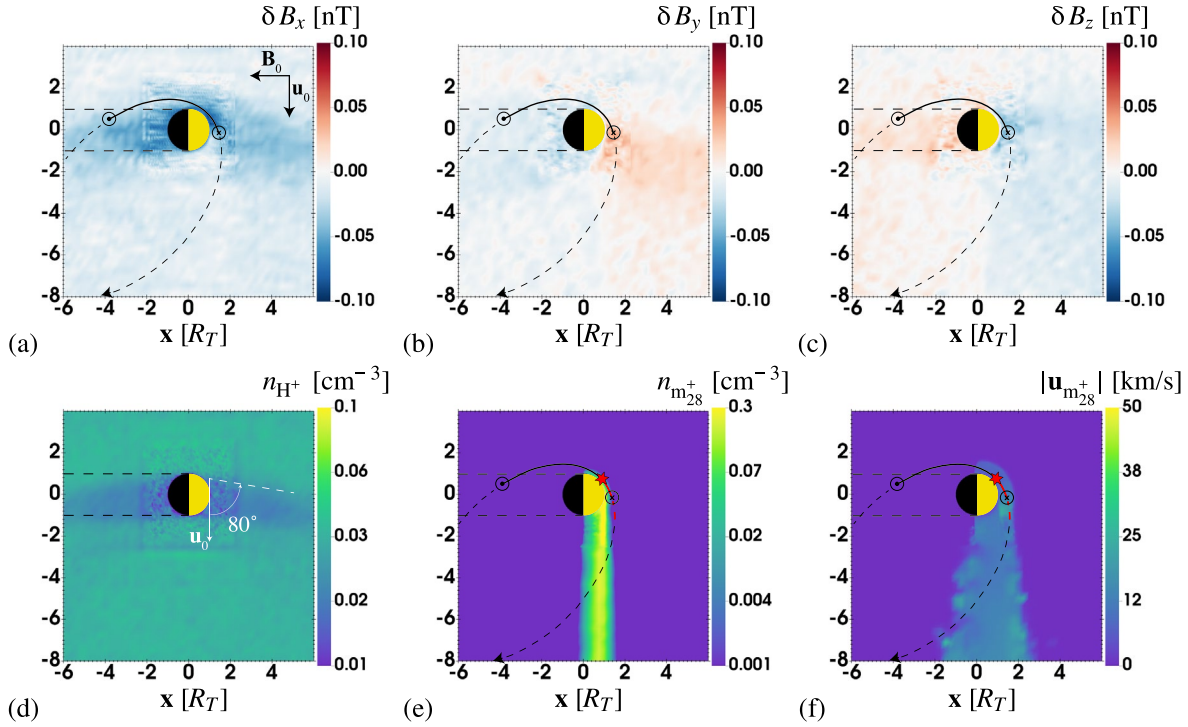

Figure 3. Model results for the June 12, 2014 encounter in the plane containing $\mathbf{B}_0$ and $\mathbf{u}_0$ (see figure (a)). The P1 trajectory is tilted ∼45° out of this plane, but for clarity, is projected with solid and dashed segments corresponding to regions above or below this plane, respectively. Horizontal dashed lines denote the lunar optical shadow. The red stars/segments in figures (e–f) mark the *observed* pickup ion burst.

of the modeled u_y enhancement is too broad, beginning ∼20 min prior to the observed signature (cf. red stars in figures 2(h–i)). This may suggest a stronger exospheric asymmetry than assumed in the model or an ionosphere that did not extend to the terminator. Regardless, the agreement between the model and observations provides strong evidence for the presence of ionospheric pickup ions generated in the Moon's dayside exosphere.

3.2. June 12, 2014: Modeling

Unlike the previous observation, the ambient flow during the June 12, 2014 encounter did *not* possess any field-aligned component (Figure 1m). Rather, the velocity was perpendicular to the background field, tilted 45° out of the SSE *x-y* plane. Since the P1 trajectory was located nearly within the *x-y* plane, ARTEMIS "missed" many features of the lunar plasma interaction (except for an enhanced pickup ion density and velocity near 14:00; Figures 1k–1n). Hence, to obtain a more comprehensive understanding of the Moon's 3D interaction with the magnetotail lobe plasma, we focus on the plane containing the ambient flow velocity and magnetic field vectors.

Figure 3 displays modeling results for the June 12, 2014 encounter. At the Moon's ramside and flanks, δB_x is enhanced (figure 3(a)), with a slight day/night asymmetry as the ambient field encounters the dayside lunar ionosphere (figure 3(e)). Figures 3(b–c) display signatures of a weakly draped magnetospheric field in δB_y and δB_z, with asymmetric perturbations on the order of 0.05 nT centered around the densest portion of the ionosphere (near $x \approx +1R_L$).

Figure 3(d) shows two regions extending from the Moon where the magnetospheric number density is reduced by a factor of ∼2 below background. Note that these are *not* signatures of the lunar Alfvén wings which, on this day, were inclined at an angle of only $\tan^{-1}\left(M_A\right) \approx 1°$ against the background field (Neubauer, 1980). Rather, these "plasma absorption wings" are generated by magnetospheric particles with large field-aligned velocities impacting the surface, creating a density depletion. Similar features have been seen at Rhea (Khurana et al., 2008; Roussos et al., 2008) and Tethys (Simon et al., 2009), forming an angle against

the flow direction of approximately $\tan^{-1}\left(u_{\text{th}} / u_0\right) \approx 80°$ (with the ambient ion thermal velocity u_{th}). Since the plasma on this day was markedly subsonic ($M_s = 0.14$), with the thermal ion velocity much higher than the bulk velocity ($u_{\text{th}} \approx 170$ km/s; $u_0 \approx 28$ km/s), any plasma wake that would form downstream of the Moon is immediately refilled by particles with large field-aligned velocities (cf. Figures 3d with 2g).

On the lunar dayside, figures 3(e–f) show that ARTEMIS again pierced through the lunar ionosphere (red stars; see also 1(k–n)). For this date, figures 3(e–f) illustrate that these particles are picked-up by the ambient magnetospheric fields and travel far ($>10R_L$) downstream of the Moon, similar to outflow of Rhea's tenuous ionosphere (Roussos et al., 2008; Teolis et al., 2010).

4. Discussion

We report the first detection of a cold ion wake extending nearly $10R_L$ downstream of the Moon when exposed to a population of tenuous, low-energy terrestrial plasma within Earth's magnetotail lobes. The tilt of this wake out of the lunar optical shadow, combined with spacecraft potential biasing, allowed for the unique opportunity to measure this otherwise invisible magnetotail lobe population. In modeling the Moon's interaction with this plasma during two ARTEMIS encounters, we have identified characteristic signatures of the lunar plasma and field environment when embedded within the lobes. These include plasma absorption wings extending from the Moon that scale with the ratio of the thermal and bulk ion velocities, and asymmetric electromagnetic perturbations generated by the disparate day/night structure of the lunar ionosphere (e.g., Halekas et al., 2018).

Within Earth's magnetotail, the Moon is exposed to an extremely low-beta, sub-Alfvénic plasma population. In this environment, an extended wake forms downstream when the ambient magnetospheric flow velocity is sufficiently aligned with the background magnetic field (e.g., Figure 2g), driven by plasma absorption at the ramside hemisphere. The reduced particle pressure within this wake is entirely compensated by a magnetic field that is slightly enhanced by ∼5%, in stark contrast to compressions of >400% when the Moon is exposed to the high beta solar wind (Poppe et al., 2014) or the magnetosheath plasma (Xu et al., 2019, 2021). Wakeside signatures similar to those at the Moon when embedded within the magnetotail lobes have been observed at Tethys and Rhea (e.g., Roussos et al., 2008; Simon et al., 2009). Near these Saturnian moons, the ambient magnetic field is nearly perpendicular to the flow velocity, the plasma is transonic ($M_s \approx 1$), and their wakeside plasma cavities extend multiple moon radii downstream (e.g., Simon et al., 2015). However, the terrestrial magnetotail lobe plasma observed here was subsonic ($M_s \ll 1$), allowing the lunar plasma cavity to be refilled at smaller distances from the surface when the magnetospheric field is perpendicular to the ambient flow velocity (e.g., Figure 3d). Despite these differences, further parallels to Saturn's moons exist since the lunar ionosphere generates electromagnetic field perturbations similar to those observed at Dione (Simon et al., 2011; Tokar et al., 2012), with ionospheric outflow similar to that observed near Rhea (Teolis et al., 2010). Hence, the ten-year-long ARTEMIS data set—expanding by ∼4 lunar encounters within the terrestrial magnetotail each month—is an invaluable resource for exploring analogous plasma parameter regimes experienced by multiple outer planet moons for which only a handful of flybys exist.

Our method to observe the low-energy terrestrial magnetotail ion population within the Moon's optical shadow can be compared to similar measurements obtained by the Geotail spacecraft in Earth's shadow (Seki et al., 2003). The unique, tilted geometry of the lunar wake with respect to the optical shadow, along with the position of ARTEMIS deep within Earth's magnetotail lobes, provides a valuable data set for observing the low-energy magnetospheric plasma population that may be related to terrestrial ionospheric outflow. Indeed, previous observations at high magnetic latitudes in the inner magnetosphere (within ≪60 Earth radii; i.e., at much closer distances to the Earth than ARTEMIS; e.g., André & Cully, 2012; Engwall, Eriksson, Cully, André, Torbert, & Vaith, 2009; Haaland et al., 2012; Su et al., 1998) can be combined with data from these recurrent ARTEMIS shadow crossings to further understand the flux and variability in the outflow of cold terrestrial plasma.

Data Availability Statement

Results are available at https://doi.org/10.5281/zenodo.4527622, with ARTEMIS data at artemis.ssl.berkeley.edu or cdaweb.gsfc.nasa.gov.

Acknowledgments
The authors are supported by NASA/LDAP Grant 80NSSC20K0311. ARTEMIS is funded and operated under NASA Grant NAS5-02099. Discussions with K.-H. Glassmeier, J.Z.D. Mieth, and U. Auster, as well as the two reviewers, have strengthened this study. We thank J.P. McFadden for use of ESA data, J.E. Bonnell and F. Mozer for use of EFI data, and K.-H. Glassmeier, U. Auster, and W. Baumjohann for the use of FGM data provided under the lead of the Technical University of Braunschweig and with financial support through the German Ministry for Economy and Technology and the German Center for Aviation and Space, Contract 50-OC-0302.

References

André, M., & Cully, C. M. (2012). Low-energy ions: A previously hidden solar system particle population. *Geophysical Research Letters*, *39*(3). https://doi.org/10.1029/2011GL050242
Angelopoulos, V. (2011). The ARTEMIS mission. *Space Science Reviews*, *165*(1–4), 3–25. https://doi.org/10.1007/s11214-010-9687-2
Arnold, H., Liuzzo, L., & Simon, S. (2020). Plasma interaction signatures of plumes at Europa. *Journal of Geophysical Research: Space Physics*, *125*(1). https://doi.org/10.1029/2019JA027346
Arnold, H., Simon, S., & Liuzzo, L. (2020). Applying ion energy spectrograms to search for plumes at Europa. *Journal of Geophysical Research: Space Physics*, *125*(9). https://doi.org/10.1029/2020JA028376
Benna, M., Mahaffy, P. R., Halekas, J. S., Elphic, R. C., & Delory, G. T. (2015). Variability of helium, neon, and argon in the lunar exosphere as observed by the LADEE NMS instrument. *Geophysical Research Letters*, *42*(10), 3723–3729. https://doi.org/10.1002/2015GL064120
Bonnell, J. W., Mozer, F. S., Delory, G. T., Hull, A. J., Ergun, R. E., Cully, C. M., et al. (2008). The electric field instrument (EFI) for THEMIS. *Space Science Reviews*, *141*(1–4), 303–341. https://doi.org/10.1007/s11214-008-9469-2
Cao, X., Halekas, J., Poppe, A., Chu, F., & Glassmeier, K. H. (2020). The acceleration of lunar ions by magnetic forces in the terrestrial magnetotail lobes. *Journal of Geophysical Research: Space Physics*, *125*(6), 1–12. https://doi.org/10.1029/2020JA027829
Choudhary, R. K., Ambili, K. M., Choudhury, S., Dhanya, M. B., & Bhardwaj, A. (2016). On the origin of the ionosphere at the Moon using results from Chandrayaan-1 S band radio occultation experiment and a photochemical model. *Geophysical Research Letters*, *43*(19), 10–25. https://doi.org/10.1002/2016GL070612
Daily, W. D., Barker, W. A., Clark, M., Dyal, P., & Parkin, C. W. (1977). Ionosphere and atmosphere of the Moon in the geomagnetic tail. *Journal of Geophysical Research*, *82*(33), 5441–5451. https://doi.org/10.1029/jb082i033p05441
Engwall, E., Eriksson, A. I., Cully, C. M., André, M., Puhl-Quinn, P. A., Vaith, H., & Torbert, R. (2009). Survey of cold ionospheric outflows in the magnetotail. *Annales Geophysicae*, *27*(8), 3185–3201. https://doi.org/10.5194/angeo-27-3185-2009
Engwall, E., Eriksson, A. I., Cully, C. M., André, M., Torbert, R., & Vaith, H. (2009). Earth's ionospheric outflow dominated by hidden cold plasma. *Nature Geoscience*, *2*(1), 24–27. https://doi.org/10.1038/ngeo387
Fatemi, S., Holmström, M., & Futaana, Y. (2012). The effects of lunar surface plasma absorption and solar wind temperature anisotropies on the solar wind proton velocity space distributions in the low-altitude lunar plasma wake. *Journal of Geophysical Research*, *117*(10). https://doi.org/10.1029/2011JA017353
Feyerabend, M., Liuzzo, L., Simon, S., & Motschmann, U. (2017). A three-dimensional model of pluto's interaction with the solar wind during the new horizons encounter. *Journal of Geophysical Research: Space Physics*, *122*(10), 10–356. https://doi.org/10.1002/2017JA024456
Georgescu, E., Plaschke, F., Auster, U., Fornaçon, K.-H., & Frey, H. U. (2011). Modelling of spacecraft spin period during eclipse. *Annales Geophysicae*, *29*(5), 875–882. https://doi.org/10.5194/angeo-29-875-2011
Haaland, S., Eriksson, A., Engwall, E., Lybekk, B., Nilsson, H., Pedersen, A., et al. (2012). Estimating the capture and loss of cold plasma from ionospheric outflow. *Journal of Geophysical Research*, *117*(7). https://doi.org/10.1029/2012JA017679
Halekas, J. S., Angelopoulos, V., Sibeck, D. G., Khurana, K. K., Russell, C. T., Delory, G. T., et al. (2011). First results from ARTEMIS, a new two-spacecraft lunar mission: Counter-streaming plasma populations in the lunar wake. *Space Science Reviews*, *165*(1–4), 93–107. https://doi.org/10.1007/s11214-010-9738-8
Halekas, J. S., Bale, S. D., Mitchell, D. L., & Lin, R. P. (2005). Electrons and magnetic fields in the lunar plasma wake. *Journal of Geophysical Research*, *110*(A7). https://doi.org/10.1029/2004JA010991
Halekas, J. S., Poppe, A. R., Delory, G. T., Sarantos, M., Farrell, W. M., Angelopoulos, V., & McFadden, J. P. (2012). Lunar pickup ions observed by ARTEMIS: Spatial and temporal distribution and constraints on species and source locations. *Journal of Geophysical Research*, *117*(6). https://doi.org/10.1029/2012JE004107
Halekas, J. S., Poppe, A. R., Delory, G. T., Sarantos, M., & McFadden, J. P. (2013). Using ARTEMIS pickup ion observations to place constraints on the lunar atmosphere. *Journal of Geophysical Research: Planets*, *118*(1), 81–88. https://doi.org/10.1029/2012JE004292
Halekas, J. S., Poppe, A. R., Harada, Y., Bonnell, J. W., Ergun, R. E., & McFadden, J. P. (2018). A tenuous lunar ionosphere in the geomagnetic tail. *Geophysical Research Letters*, *45*(18), 9450–9459. https://doi.org/10.1029/2018GL079936
Harada, Y., Machida, S., Halekas, J. S., Poppe, A. R., & McFadden, J. P. (2013). ARTEMIS observations of lunar dayside plasma in the terrestrial magnetotail lobe. *Journal of Geophysical Research: Space Physics*, *118*(6), 3042–3054. https://doi.org/10.1002/jgra.50296
Hodges, R. R. (1975). Formation of the lunar atmosphere. *The Moon*, *14*(1), 139–157. https://doi.org/10.1007/BF00562980
Hodges, R. R., Hoffman, J. H., & Johnson, F. S. (1974). The lunar atmosphere. *Icarus*, *21*(4), 415–426. https://doi.org/10.1016/0019-1035(74)90144-4
Imamura, T., Nabatov, A., Mochizuki, N., Iwata, T., Hanada, H., Matsumoto, K., et al. (2012). Radio occultation measurement of the electron density near the lunar surface using a subsatellite on the SELENE mission. *Journal of Geophysical Research*, *117*(6). https://doi.org/10.1029/2011JA017293
Kallio, E. (2005). Formation of the lunar wake in quasi-neutral hybrid model. *Geophysical Research Letters*, *32*(6), L06107. https://doi.org/10.1029/2004GL021989
Khurana, K. K., Fatemi, S., Lindkvist, J., Roussos, E., Krupp, N., Holmström, M., et al. (2017). The role of plasma slowdown in the generation of Rhea's Alfvén wings. *Journal of Geophysical Research: Space Physics*, *122*(2), 1778–1788. https://doi.org/10.1002/2016JA023595
Khurana, K. K., Russell, C. T., & Dougherty, M. K. (2008). Magnetic portraits of Tethys and Rhea. *Icarus*, *193*(2), 465–474. https://doi.org/10.1016/j.icarus.2007.08.005
Krupp, N., Kotova, A., Roussos, E., Simon, S., Liuzzo, L., Paranicas, C., et al. (2020). Magnetospheric interactions of Saturn's Moon Dione (2005–2015). *Journal of Geophysical Research: Space Physics*, *125*(6). https://doi.org/10.1029/2019JA027688
Liuzzo, L., Simon, S., & Feyerabend, M. (2018). Observability of Callisto's inductive signature during the JUpiter ICy Moons explorer mission. *Journal of Geophysical Research: Space Physics*, *123*(11), 9045–9054. https://doi.org/10.1029/2018JA025951

Liuzzo, L., Simon, S., Feyerabend, M., & Motschmann, U. (2017). Magnetic signatures of plasma interaction and induction at Callisto: The Galileo C21, C22, C23, and C30 flybys. *Journal of Geophysical Research: Space Physics*, *122*(7), 7364–7386.

Liuzzo, L., Simon, S., & Regoli, L. (2019a). Energetic electron dynamics near Callisto. *Planetary and Space Science*, *179*, 104726. https://doi.org/10.1016/j.pss.2019.104726

Liuzzo, L., Simon, S., & Regoli, L. (2019b). Energetic ion dynamics near Callisto. *Planetary and Space Science*, *166*, 23–53. https://doi.org/10.1016/j.pss.2018.07.014

McFadden, J. P., Carlson, C. W., Larson, D., Bonnell, J., Mozer, F., Angelopoulos, V., et al. (2008). THEMIS ESA first science results and performance issues. *Space Science Reviews*, *141*(1–4), 477–508. https://doi.org/10.1007/s11214-008-9433-1

McFadden, J. P., Carlson, C. W., Larson, D., Ludlam, M., Abiad, R., Elliott, B., et al. (2008). The THEMIS ESA plasma instrument and in-flight calibration. *Space Science Reviews*, *141*(1–4), 277–302. https://doi.org/10.1007/s11214-008-9440-2

Michel, F. C. (1968). Lunar wake at large distances. *Journal of Geophysical Research*, *73*(23), 7277–7283. https://doi.org/10.1029/JA073i023p07277

Müller, J., Simon, S., Motschmann, U., Schüle, J., Glassmeier, K.-H., & Pringle, G. J. (2011). A.I.K.E.F.: Adaptive hybrid model for space plasma simulations. *Computer Physics Communications*, *182*(4), 946–966. https://doi.org/10.1016/j.cpc.2010.12.033

Ness, N. F. (1965). The magnetohydrodynamic wake of the Moon. *Journal of Geophysical Research*, *70*(3), 517–534. https://doi.org/10.1029/JZ070i003p00517

Neubauer, F. M. (1980). Nonlinear standing Alfvén wave current system at Io: Theory. *Journal of Geophysical Research*, *85*(9), 1171–1178. https://doi.org/10.1029/JA085iA03p01171

Ogilvie, K. W., Steinberg, J. T., Fitzenreiter, R. J., Owen, C. J., Lazarus, A. J., Farrell, W. M., & Torbert, R. B. (1996). Observations of the lunar plasma wake from the WIND spacecraft on December 27, 1994. *Geophysical Research Letters*, *23*(10), 1255–1258. https://doi.org/10.1029/96GL01069

Poppe, A. R., Fatemi, S., Halekas, J. S., Holmström, M., & Delory, G. T. (2014). ARTEMIS observations of extreme diamagnetic fields in the lunar wake. *Geophysical Research Letters*, *41*(11), 3766–3773. https://doi.org/10.1002/2014GL060280

Poppe, A. R., Halekas, J. S., Samad, R., Sarantos, M., & Delory, G. T. (2013). Model-based constraints on the lunar exosphere derived from ARTEMIS pickup ion observations in the terrestrial magnetotail. *Journal of Geophysical Research: Planets*, *118*(5), 1135–1147. https://doi.org/10.1002/jgre.20090

Poppe, A. R., Samad, R., Halekas, J. S., Sarantos, M., Delory, G. T., Farrell, W. M., et al. (2012). ARTEMIS observations of lunar pick-up ions in the terrestrial magnetotail lobes. *Geophysical Research Letters*, *39*(17). https://doi.org/10.1029/2012GL052909

Potter, A. E., & Morgan, T. H. (1988, 8). Discovery of sodium and potassium vapor in the atmosphere of the Moon. *Science*, *241*(4866), 675–680. https://doi.org/10.1126/science.241.4866.675

Roussos, E., Müller, J., Simon, S., Bößwetter, A., Motschmann, U., Krupp, N., et al. (2008). Plasma and fields in the wake of Rhea: 3-D hybrid simulation and comparison with Cassini data. *Annales Geophysicae*, *26*(3), 619–637. https://doi.org/10.5194/angeo-26-619-2008

Sarantos, M., Hartle, R. E., Killen, R. M., Saito, Y., Slavin, J. A., & Glocer, A. (2012). Flux estimates of ions from the lunar exosphere. *Geophysical Research Letters*, *39*(13). https://doi.org/10.1029/2012GL052001

Saur, J., Neubauer, F. M., & Schilling, N. (2007). Hemisphere coupling in Enceladus' asymmetric plasma interaction. *Journal of Geophysical Research*, *112*, A11209. https://doi.org/10.1029/2007JA012479

Seki, K., Hirahara, M., Hoshino, M., Terasawa, T., Elphic, R. C., Saito, Y., et al. (2003). Cold ions in the hot plasma sheet of Earth's magnetotail. *Nature*, *422*(6932), 589–592. https://doi.org/10.1038/nature01502

Simon, S., Kriegel, H., Saur, J., Wennmacher, A., Neubauer, F. M., Roussos, E., et al. (2012). Analysis of Cassini magnetic field observations over the poles of Rhea. *Journal of Geophysical Research*, *117*(A7). https://doi.org/10.1029/2012JA017747

Simon, S., Roussos, E., & Paty, C. S. (2015). The interaction between Saturn's moons and their plasma environments. *Physics Reports*, *602*, 1–65. https://doi.org/10.1016/j.physrep.2015.09.005

Simon, S., Saur, J., Neubauer, F. M., Motschmann, U., & Dougherty, M. K. (2009). Plasma wake of Tethys: Hybrid simulations versus Cassini MAG data. *Geophysical Research Letters*, *36*(4), L04108. https://doi.org/10.1029/2008GL036943

Simon, S., Saur, J., Neubauer, F. M., Wennmacher, A., & Dougherty, M. K. (2011). Magnetic signatures of a tenuous atmosphere at Dione. *Geophysical Research Letters*, *38*, L15102. https://doi.org/10.1029/2011GL048454

Stern, S. A. (1999). The lunar atmosphere: History, status, current problems, and context. *Reviews of Geophysics*, *37*(4), 453–491. https://doi.org/10.1029/1999RG900005

Su, Y.-J., Horwitz, J. L., Moore, T. E., Giles, B. L., Chandler, M. O., Craven, P. D., et al. (1998). Polar wind survey with the thermal ion dynamics experiment/plasma source instrument suite aboard POLAR. *Journal of Geophysical Research*, *103*(A12), 29305–29337. https://doi.org/10.1029/98JA02662

Tanaka, T., Saito, Y., Yokota, S., Asamura, K., Nishino, M. N., Tsunakawa, H., et al. (2009). First in situ observation of the Moon-originating ions in the Earth's magnetosphere by MAP-PACE on SELENE (KAGUYA). *Geophysical Research Letters*, *36*(22), 1–5. https://doi.org/10.1029/2009GL040682

Teolis, B. D., Jones, G. H., Miles, P. F., Tokar, R. L., Magee, B. A., Waite, J. H., et al. (2010). Cassini finds an oxygen-carbon dioxide atmosphere at Saturn's icy Moon Rhea. *Science*, *330*(6012), 1813–1815. https://doi.org/10.1126/science.1198366

Tokar, R. L., Johnson, R. E., Thomsen, M. F., Sittler, E. C., Coates, A. J., Wilson, R. J., et al. (2012). Detection of exospheric O2+ at Saturn's moon Dione. *Geophysical Research Letters*, *39*(3), L03105. https://doi.org/10.1029/2011GL050452

Travnicek, P., Hellinger, P., Schriver, D., Bale, S. D., Trávníček, P., Hellinger, P., et al. (2005). Structure of the lunar wake: Two-dimensional global hybrid simulations. *Geophysical Research Letters*, *32*(6), L06102. https://doi.org/10.1029/2004GL022243

Vernisse, Y., Kriegel, H., Wiehle, S., Motschmann, U., & Glassmeier, K.-H. (2013). Stellar winds and planetary bodies simulations: Lunar type interaction in super-Alfvénic and sub-Alfvénic flows. *Planetary and Space Science*, *84*, 37–47. https://doi.org/10.1016/j.pss.2013.04.004

Wiehle, S., Plaschke, F., Motschmann, U., Glassmeier, K.-H., Auster, H. U., Angelopoulos, V., et al. (2011). First lunar wake passage of ARTEMIS: Discrimination of wake effects and solar wind fluctuations by 3D hybrid simulations. *Planetary and Space Science*, *59*(8), 661–671. https://doi.org/10.1016/j.pss.2011.01.012

Xu, X., Xu, J., Xu, Q., Chang, Q., & Wang, J. (2021). Rapid refilling of the lunar wake under transonic plasma flow: ARTEMIS observations. *Acta Pathologica Japonica*, *908*(2), 227. https://doi.org/10.3847/1538-4357/abd6f1

Xu, X., Xu, Q., Chang, Q., Xu, J., Wang, J., Wang, Y., et al. (2019). ARTEMIS observations of well-structured lunar wake in subsonic plasma flow. *Acta Pathologica Japonica*, *881*(1), 76. https://doi.org/10.3847/1538-4357/ab2e0a

Zhang, H., Khurana, K. K., Kivelson, M. G., Angelopoulos, V., Wan, W. X., Liu, L. B., et al. (2014). Three-dimensional lunar wake reconstructed from ARTEMIS data. *Journal of Geophysical Research: Space Physics*, *119*(7), 5220–5243. https://doi.org/10.1002/2014JA020111

Zhou, X.-Z., Angelopoulos, V., Poppe, A. R., & Halekas, J. S. (2013). ARTEMIS observations of lunar pickup ions: Mass constraints on ion species. *Journal of Geophysical Research: Planets*, *118*(9), 1766–1774. https://doi.org/10.1002/jgre.20125

Zhou, X.-Z., Angelopoulos, V., Poppe, A. R., Halekas, J. S., Khurana, K. K., Kivelson, M. G., et al. (2014). Lunar dayside current in the terrestrial lobe: ARTEMIS observations. *Journal of Geophysical Research: Space Physics*, *119*(5), 3381–3391. https://doi.org/10.1002/2014JA019842